PNAS
www.pnas.org

Supplementary Information for

Pharmacological reactivation of inactive X-linked *Mecp2* in cerebral cortical neurons of living mice

Piotr Przanowski, Urszula Wasko, Zeming Zheng, Jun Yu, Robyn Sherman, Lihua Julie Zhu, Michael J. McConnell, Jogender Tushir-Singh, Michael R. Green and Sanchita Bhatnagar

Sanchita Bhatnagar
Email: sb5fk@virginia.edu

Michael R. Green
Email: michael.green@umassmed.edu

This PDF file includes:

Supplementary text
Figs. S1 to S6
Tables S1 to S2
References for SI reference citations

www.pnas.org/cgi/doi/10.1073/pnas.1803792115

Supplementary Information Text

SI Materials and Methods

Cell Culture and Mice. H4SV cells (1) and BMSL2 (HOBMSL2, (2)) cells were cultured as recommended by the supplier. Human iPSCs (provided by Maria C.N. Marchetto, The Salk Institute for Biological Studies, La Jolla) were expanded, NPCs were generated by dual SMAD inhibition, and mature neurons derived as described previously (3).

Mouse strains used in the study were obtained as follows: *Xist/ΔXist* (B6;129-Xist<tm5Sado>, provided by Antonio Bedalov, Fred Hutchinson Cancer Research Center, Seattle), *Mecp2*$^{tm3.1Bird}$/J (Jackson Laboratory), *Stc1-/-* (provided by David Sheikh-Hamad, Baylor College of Medicine, Houston), and *Mecp2-Gfp/Mecp2-Gfp* (Jackson Laboratory). Work involving mice adhered to the guidelines of the University of Virginia Institutional Animal Care and Use Committee (IACUC) protocol no. 4112. MEFs were isolated from female *XistΔ:Mecp2/Xist:Mecp2-Gfp* embryos at embryonic day 15.5 (E15.5) obtained from *Xist/ΔXist* female mice crossed with *Mecp2-Gfp/Y* male mice. Embryos and MEFs were isolated as described previously (4), and were PCR-genotyped using gene-specific primers listed in Table S1. *XistΔ:Mecp2/Xist:Mecp2-Gfp* mice were generated by crossing male *Xist:Mecp2-Gfp/Y* mice (5) with female *XistΔ:Mecp2/Xist:Mecp2* mice (6), and were PCR-genotyped using gene-specific primers listed in Table S1.

Mouse Cortex Dissection, Nuclei Isolation, Staining and Flow Cytometry. Mouse cortexes were isolated and frozen, as described previously (7). Isolated cortexes were fixed by homogenization in NIM buffer (250 mM sucrose, 25 mM KCl, 5 mM $MgCl_2$, 10 mM Tris-Cl) supplemented with 2% PFA and 0.1% Triton X-100. Nuclei were pelleted and resuspended in NIM buffer supplemented with 25% ladixinol and purified by gradient separation (29% ladixinol). Nuclei were stained with anti-RBFOX3/NeuN (1B7) (Novus) and 7-AAD (Biolegend). Flow cytometry analysis was performed on the Cytek FACS Calibur Benchtop Analyzers (Becton Dickinson) at University of Virginia Flow Cytometry Core.

Chemical Inhibitor Treatment. Female mouse fibroblasts were treated with small molecule inhibitors at the following concentrations: 0.5 μM LDN193189 (Cayman Chemical), 0.5 μM dorsomorphin (Cayman Chemical), 0.5 μM K02288 (Cayman Chemical), 0.5 μM rapamycin (Cayman Chemical), 0.5 μM everolimus (Cayman Chemical), 0.5 μM KU-0063794 (Apex Bio) and 2.5 μM GSK650394 (Apex Bio) for ~2 weeks. Medium containing fresh inhibitors was exchanged every 2 days. *XistΔ:Mecp2/Xist:Mecp2-Gfp* MEFs were treated with 2.5 μM GSK650394 and 0.5 μM LDN193189 for ~2 weeks. RTT-neurons were treated with 2.5 μM GSK650394 and 0.5 μM LDN193189 for 3 weeks and the half-medium change was done every 3 days. For synergy experiments, the Bliss score, an index of drug cooperativity (8), was calculated. Bliss score greater than 0 for the drug combination indicatives synergistic effect.

Mouse Brain Injections, Brain Isolation and Sectioning. Chemical inhibitors (1.5 mM LDN193189 and 1.6 mM GSK650394) were re-suspended in vehicle (0.9% NaCl, 0.5% methylcelulose, 4.5% DMSO), or vehicle alone was injected into the opposite hemispheres of the brain of an anesthetized mouse every 2 days for 21 days. The drug regimen was based on the results from the rate of reactivation achieved in RTT-neurons. To maintain spatiotemporal control, all injections were done approximately at the predefined stereotactic coordinates with the position of bregma set as the reference of the X and Y coordinates (stereotactic zero). At the termination of the experiment, mice were sacrificed, and fixed by transcardial perfusion with 4% paraformaldehyde. Mouse brains were then isolated, embedded in Optimum Cutting Temperature (OCT) and frozen at -80^{o}C. Cryo-sectioning was performed at University of Virginia Histology core. Sections were mounted and analyzed by immunofluorescence as described below.

Immunofluorescence, Quantitative Immunofluorescence and RNA FISH. H4SV cells and MEFs were stained with an anti-GFP primary antibody (1:100, Cell Signaling) as described previously (7). Neurons and brain sections were subjected to antigen retrieval (0.1 M citric acid, 0.1 M Tris-base, pH=6; 5 min in 100°C)

before staining. Neurons were stained with an anti-MAP2 (1:1000, Aves Labs, MAP) and an anti-β-III-tubulin (TUBB3; 1:250, Biolegend, 657405). Brain sections were stained with an anti-GFP antibody. Quantitative immunofluorescence was done to measure the GFP intensity in the drug treated *XistΔ:Mecp2/Xist:Mecp2-Gfp* MEFs as described previously (9).

RNA FISH experiments were performed as described previously (7). Cells were visualized on a Zeiss AxioObserver Live-Cell microscope and images were adjusted for contrast and brightness using AxioVision Software. For quantification, 100–500 cells in at least 10 different fields were counted and scored for positive signal. Fluorescence levels in MEFs and neuronal morphological features were measured using ImageJ software.

qRT-PCR. Total RNA was isolated by TRIzol Reagent (Life Technologies) and reverse transcribed using ProtoScript Reverse Transcriptase (New England Biolabs). qRT-PCR was performed as described previously (7) using primers listed in Table S1. For allele-specific analysis of *MECP2* in RTT-neurons, cDNA was synthesized from the total RNA as described previously (7) and the wild-type and mutant *MECP2* transcripts were amplified using specific Taqman probes (rs28934906, Applied Biosystems). The expression level for all genes was normalized to the house-keeping gene *Gapdh.* The expression level of wild-type MECP2 in control neurons expressing wild-type MECP2 from the Xa was set to 100% and the background from RTT-neurons was set to 0%.

ChIP Assays. The SMAD- and YY1-binding motifs in the *Xist* promoter were identified using Gene Promoter Miner software (10) and are shown in Table S2. ChIP assays were performed as described previously (7) using antibodies against tri-methyl-histone H3 (Lys4) (Cell Signaling), YY1 (Santa Cruz), H2A-ub (Cell Signaling), H3K27me3 (Cell Signaling) and ph-Smad1/3/5 (Cell Signaling). ChIP products were analyzed by qPCR using primers listed in Table S1. Primers targeting a gene desert region in chromosome 14-97450841 were used as a negative control. The results are presented as percentage of input material immunoprecipitated and normalized to an IgG control.

***Xist* RNA Stability Assay.** The assay was performed as described previously (7). After treatment with DNase (Ambion), *Xist* RNA levels, and as a control *Gapdh*, were quantified by qRT-PCR using primers listed in Table S1.

Immunoblotting. Cell extracts were prepared by lysing cell pellet in RIPA buffer supplemented with 1 mM sodium ortho-vanadate and 10 mM PMSF. To prepare protein extract from mouse brain or liver tissue, tissue was homogenized in lysis buffer (1% SDS, 1 mM sodium ortho-vanadate, 10 mM Tris-Cl, pH 7.4 and protease inhibitor). Immunoblots were probed using antibodies against ph-Smad1/3/5 (Cell Signaling), SMAD (Cell Signaling), ph-MDM2 (Cell Signaling), MDM2 (Cell Signaling), ph-p70S6k (Cell Signaling), p70S6k (Cell Signaling), and α-tubulin (Invitrogen).

Neuronal Morphological Quantification. Neuronal morphological features were quantified using the image analysis software Cell Profiler (11).

MTT Cell Proliferation Assay. MTT was performed using a MTT Cell Proliferation Assay Kit (Trevigen) according to the manufacturer's instructions.

Statistical analysis. All experiments were performed in at least triplicate and the results presented are the mean of three different biological replicates. The comparisons between the two groups were done by unpaired *t*-test; comparisons between multiple treatment groups were done by one-way or two-way ANOVA with indicated multiple comparisons *post hoc* tests. All statistical analyses were performed using R/Bioconductor (version 2.15.2).

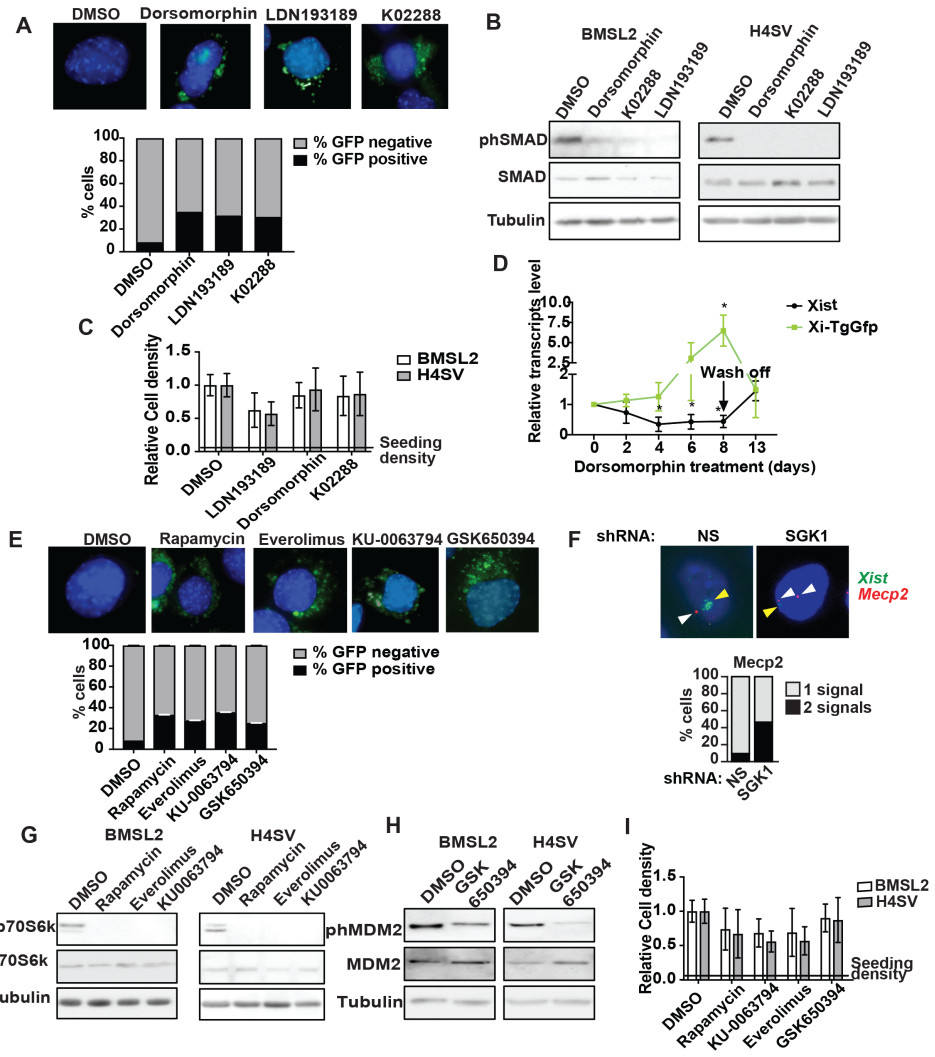

Fig. S1. Reactivation of Xi-linked genes by small molecule inhibitors of ACVR1, mTOR and SGK1. (*A*) Immunofluorescence monitoring expression of GFP (green) in H4SV cells treated with DMSO or an ACVR1 inhibitor. DAPI staining is shown in blue. Representative images are shown (*Upper*), and the results quantified (*Lower*). (*B*) Immunoblot monitoring the levels of phosphorylated SMAD (phSMAD) and total SMAD in BMSL2 (*Left*) and H4SV (*Right*) cells treated with DMSO or an ACVR1 inhibitor. Tubulin was monitored as a loading control. The results show that each ACVR1 inhibitor efficiently inhibited BMP signaling, as determined by a reduction in phSMAD a downstream effector of ACVR1. (*C*) Cellular viability of BMSL2 and H4SV cells as monitored by MTT following treatment with DMSO or an ACVR1 inhibitor. The results were normalized to that obtained with DMSO, which was set to 1. The black line indicates the seeding density. (*D*) qRT-PCR monitoring expression of *Xist* (black) and Xi-*TgGfp* (green) in H4SV cells treated with dorsomorphin, and for 5 days following removal of the inhibitor. The results were normalized to that obtained at day 0, which was set to 1. Error bars indicate SD, * $p<0.05$. (*E* and *F*) Immunofluorescence monitoring expression of GFP (green) in H4SV cells treated with DMSO, mTOR inhibitor or SGK1 inhibitor (*E*), or RNA-FISH monitoring the expression of *Mecp2* and *Xist* in cells expressing a non-silencing (NS) or SGK1 shRNA (*F*). DAPI staining is shown in blue. Representative images are shown (*Upper*) and the results quantified (*Lower*). (*G*) Immunoblot monitoring levels of phosphorylated p70S6K (ph-p70S6K) or total p70S6K in BMSL2 (*Left*) and H4SV cells (*Right*) following treatment with DMSO or an mTOR inhibitor. The results show that the mTOR inhibitors blocked phosphorylation of p70S6K, a downstream effector of mTOR. (*H*) Immunoblot monitoring levels of phosphorylated MDM2 (ph-MDM2) or total MDM2 in BMSL2 (*Left*) and H4SV cells (*Right*) following

treatment with DMSO or the SGK1 inhibitor GSK650394. The results show that the SGK1 inhibitor blocked phosphorylation of MDM2, a downstream effector of SGK1. (*I*) Relative cell viability, as monitored by MTT, of H4SV and BMSL2 cells treated with DMSO, rapamycin, KU-0063794, everolimus or GSK650394. The results were normalized to that obtained with DMSO, which was set to 1. The black line indicates the seeding density. Error bars indicate SD.

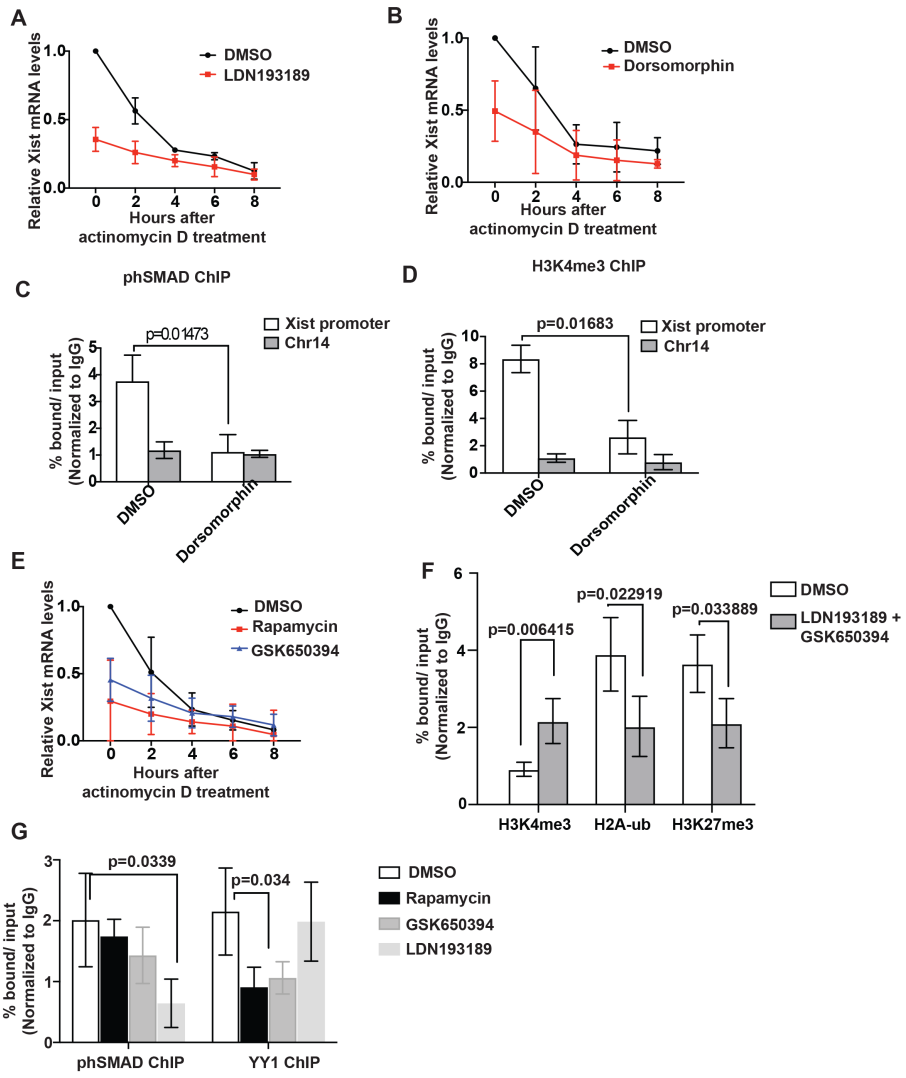

Fig. S2. Transcriptional regulation of *Xist* by small molecule ACVR1, mTOR and SGK1 inhibitors. (*A* and *B*) qRT-PCR analysis monitoring *Xist* mRNA levels in H4SV cells treated with DMSO or LDN193189 (*A*) or dorsomorphin (*B*) following treatment with actinomycin D. *Gapdh* mRNA was used as a normalization control. The results were normalized to that obtained in DMSO-treated cells prior to actinomycin D treatment, which was set to 1. (*C* and *D*) ChIP analysis monitoring binding of phosphorylated SMAD (phSMAD) (*C*) and H3K4me3 (*D*) on the *Xist* promoter and, as a negative control, a region on chromosome 14 (Chr14) in H4SV cells treated with DMSO or dorsomorphin. (*E*) qRT-PCR analysis monitoring *Xist* levels in H4SV cells treated with DMSO, rapamycin or GSK650394 following treatment with actinomycin D. *Gapdh* mRNA was used as a normalization control. (*F*) ChIP analysis monitoring binding of H3K4me3, H2A-ub and H3K27me3 on the Xi-linked *Gfp* promoter in H4SV cells treated with DMSO or LDN193189 and GSK650394. (*G*) ChIP analysis monitoring binding of phSMAD and YY1 on the *Xist* promoter in H4SV cells treated with DMSO, rapamycin, GSK650394 or LDN193189. Error bars indicate SD.

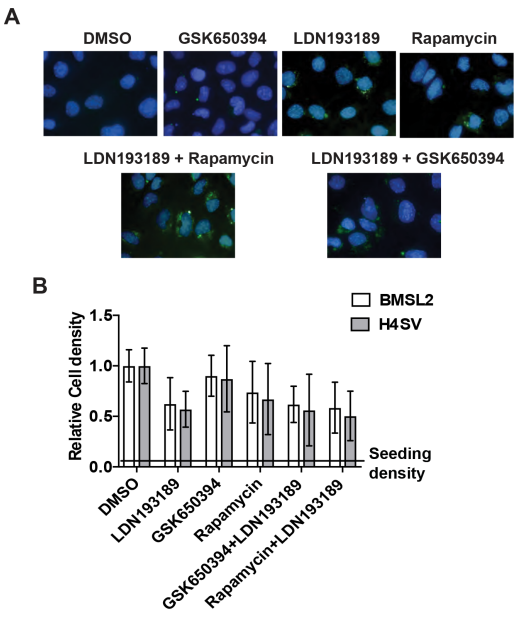

Fig. S3. Inhibitors of ACVR1 and PDPK1 effectors synergistically reactivate Xi-linked genes and do not adversely affect cellular proliferation. (*A*) Representative immunofluorescence images showing GFP expression in H4SV cells treated with DMSO, GSK650394, LDN193189 or rapamycin either alone or in combination. DAPI staining is shown in blue. (*B*) Cellular viability monitored by MTT, of H4SV and BMSL2 cells treated with DMSO, LDN193189, GSK650394, or rapamycin either alone or in combination. The results were normalized to that obtained with DMSO, which was set to 1. The black line indicates the seeding density at day 0. Error bars indicate SD.

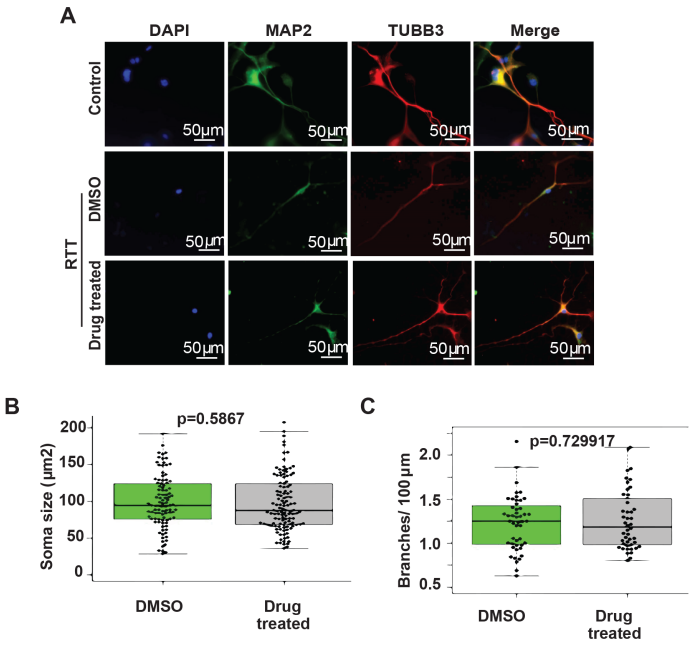

Fig. S4. Inhibitors of ACVR1 and PDPK1 effectors alter neuronal morphology of RTT neurons but not control neurons. (*A*) Representative immunofluorescence images showing neuronal morphology of control neurons or RTT neurons treated with either DMSO or drug. Scale bar, 50 µm. Quantitative analysis of soma cross-sectional area (*B*) and number of neuronal branch points (*C*) in MAP2+ control neurons treated with DMSO or drug combination. Each dot represents one neuron.

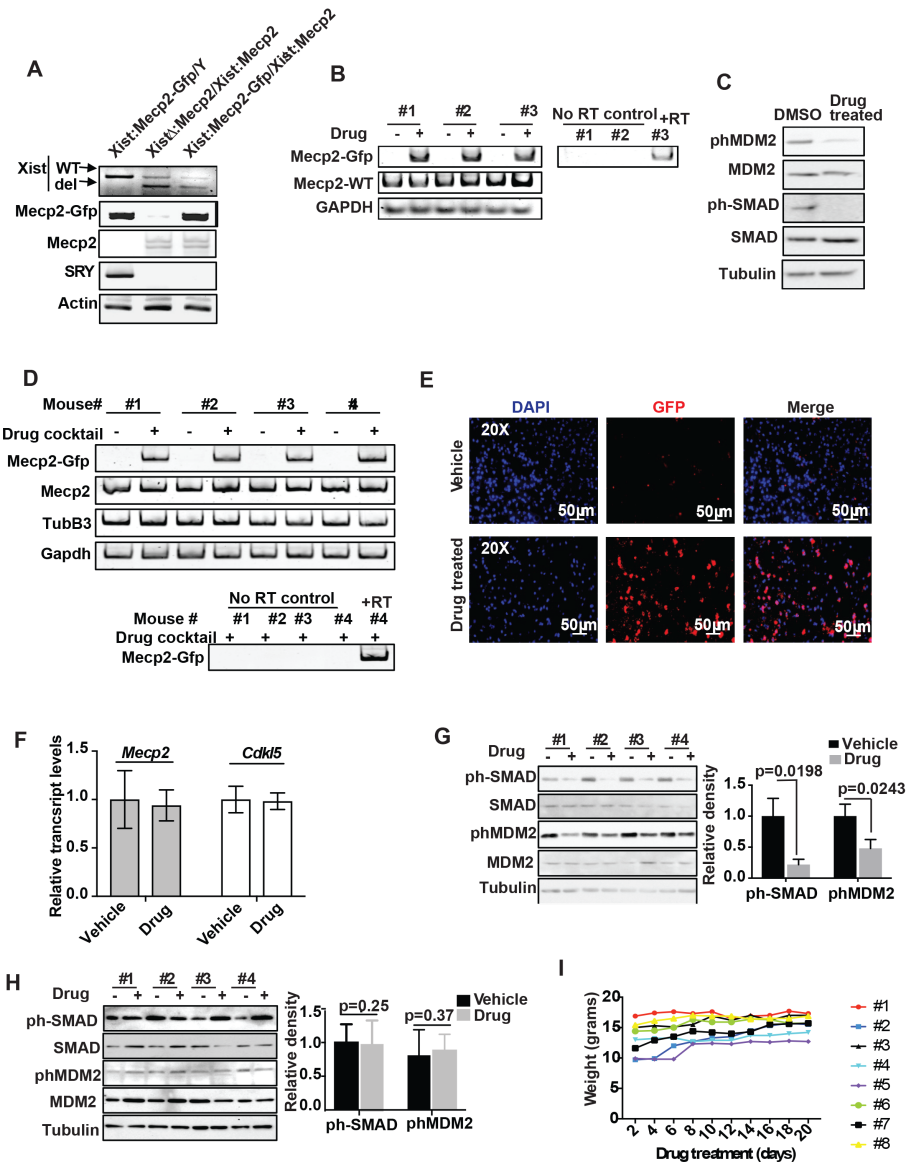

Fig. S5. Pharmacological reactivation of X-linked *Mecp2* in the brain of female *XistΔ:Mecp2/Xist:Mecp2-Gfp* mice. (*A*) PCR genotyping of *Xist:Mecp2-Gfp/Y*, *XistΔ:Mecp2/Xist:Mecp2* and *XistΔ:Mecp2/Xist:Mecp2-Gfp* mice. Mice were monitored for the presence of Mecp2-Gfp, Mecp2 and SRY. Actin was used as a loading control. (*B*) RT-PCR analysis monitoring expression of the *Mecp2-Gfp* and wild-type *Mecp2* transcripts in female *XistΔ:Mecp2/Xist:Mecp2-Gfp* MEFs following treatment with DMSO or drug (LDN193189 and GSK650394). *Gapdh* was monitored as a loading control. No RT was used as a control to rule out DNA contamination. (*C*) Immunoblot showing levels of phosphorylated and total MDM2 and SMAD in female *XistΔ:Mecp2/Xist:Mecp2-Gfp* MEFs treated with DMSO or drug combination. Tubulin was monitored as a loading control. (*D*) RT-PCR analysis monitoring expression of *Mecp2-Gfp* and *Mecp2* in vehicle- or drug-infused brain hemispheres (n=4) using *Mecp2-Gfp* and wild-type *Mecp2* specific primers. *TubB3* and *Gapdh* specific primers were used as endogenous controls. No RT was used as a control to rule out DNA contamination. (*E*) Representative immunofluorescence images of coronal brain sections of female *XistΔ:Mecp2/Xist:Mecp2-Gfp* mice injected with vehicle or drug and immunostained with an anti-GFP antibody (red). DAPI staining is shown in blue. The results confirm expression of *Xi-Mecp2-Gfp* using an anti-GFP antibody, thereby ruling out the possibility of auto-fluorescence of the small molecule inhibitors. (*F*) qRT-PCR

analysis monitoring relative transcript levels of *Mecp2* and *Cdkl5* (another X-linked gene) in vehicle- or drug (LDN193189 and GSK650394)-treated hemispheres of female *XistΔ:Mecp2/Xist:Mecp2-Gfp* mice (n=4). The results show that the total levels of *Mecp2* and *Cdkl5* do not significantly change following drug treatment, consistent with the existence of a compensatory mechanism that prevents an increase in total X-linked gene expression in cells with defective XCI (see Discussion). (*G* and *H*) Immunoblot showing levels of phosphorylated and total MDM2 and SMAD in vehicle- or drug-infused hemispheres (*G*; n=4) and liver tissue lysates (*H*; n=4) of female *XistΔ:Mecp2/Xist:Mecp2-Gfp* mice. Tubulin was monitored as a loading control. The quantitation of the knockdown for phSMAD and phMDM2 is shown. (*I*) Body weight of female *XistΔ:Mecp2/Xist:Mecp2-Gfp* mice treated by vehicle- or drug-infusion in brain hemispheres (n=8). Error bars indicate SD.

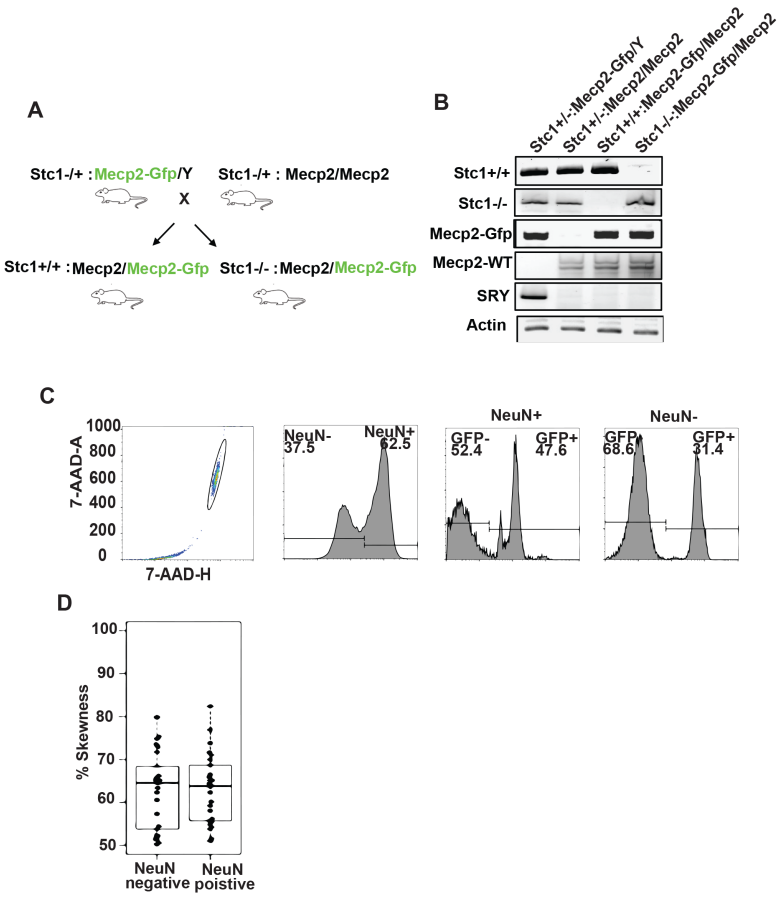

Fig. S6. Genetic rescue of Xi-linked *Mecp2* in *Stc1-/-* mice. (*A*) Schematic of breeding strategy for generating *Stc1-/-:Mecp2/Mecp2-Gfp* and *Stc1+/+:Mecp2/Mecp2-Gfp* mice. (*B*) PCR genotyping of *Stc1+/-:Mecp2-Gfp/Y*, *Stc1+/-:Mecp2/Mecp2*, *Stc1+/+: Mecp2-Gfp/Mecp2* and *Stc1-/-:Mecp2-Gfp/Mecp2*. The presence of Stc1, Mecp2-Gfp and SRY were monitored. Actin was monitored as a loading control. (*C*) A gating strategy for GFP analysis of nuclei isolated from the mouse brain by flow cytometry. Single nuclei were gated based on forward and side scatter. NeuN+ and NeuN- brain cells were selected and examined for GFP expression. *(D*) Distribution of the skewness of XCI in NeuN+ and NeuN- brain cells isolated from *Mecp2/Mecp2-Gfp* mice.

Table S1. List of primers used for qRT-PCR, allele-specific qRT-PCR, ChIP assays and mouse genotyping.

	Forward primer (5' -> 3')	**Reverse primer (5' -> 3')**
qRT-PCR		
Xist	CCCTGCTAGTTTCCCAATGA	GGAATTGAGAAAGGGCACAA
Gapdh	TGCACCACCAACTGCTTAGC	GGCATGGACTGTGGTCATGAG
GFP	GCACAATAACCAGCACGTTG	GCCTCTGCTAACCATGTTCATG
Mecp2-GFP	CCAAACAGAGAGGAGCCTGTG	GCTGAACTTGTGGCCGTTTA
Mecp2-WT	CCAAACAGAGAGGAGCCTGTG	TGTCAGAGCCCTACCCATAAG
TubB3	ATGGACAGTGTTCGGTCTGG	TCCGCACGACATCTAGGACT
Cdkl5	TTCGCATTCACTGTCTGCAC	AAGAGCTGCAAACTGTTGGC
ChIP		
Xist(SMAD)	ATTCATGGGACGCCTAAAGGG	TTGTCTCGTTGATTCACGCTG
Xist(H3K4me3)	TAAAGGTCCAATAAGATGTCAGAA	GGAGAGAAACCACGGAAGAA
Xist(YY1)	GCTCGACAGCCCAATCTTTG	AGAACTTGAGCCGCCATCTT
Chr14-97450841	CAATGCATGGGTCCAGATTT	ATTGGCACGGAAGTAGTGCT
Mouse genotyping		
Stc1-WT	AGCGCACGAGGCGGAACAAA	AGAGAGCCGCTGTGAGGCGT
Stc1-KO	AAAAGCCAGAGGTGCAAGAA	TATGATCGGAATTCCTCGAC
Xist-WT	CGGGGCTTGGTGGATGGAAAT	GCACAACCCCGCAAATGCTA
Xist-KO	GGTCCCTCGAAGAGGTTCACTAG	GCACAACCCCGCAAATGCTA
Mecp2-WT	AACAGAGAGGAGCCTGTGGA	AATTGCCCTAACGAGCACAC
Mecp2-GFP	AACAGAGAGGAGCCTGTGGA	GAACTTCAGGGTCAGCTTGC
Sry	TTGTCTAGAGAGCATGGAGGGCCATGT	CTCCTCTGTGACACTTTAGCCCTCCGA

Table S2. List of putative SMAD- and YY1-binding sites in the promoter region (-1500 to +1500 bp) of *Xist*.

TRANSFAC motif	Position of motif relative to *Xist* TSS	Strand
YY1_01	-317	-
YY1_01	-136	+
YY1_01	+74	+
YY1_01	+743	-
YY1_01	+1206	-
YY1_Q6	-412	+
YY1_Q6	+15	+
YY1_Q6	+1261	-
YY1_Q6	+1357	-
YY1_Q6	+1470	-
SMAD_Q6	-756	+
SMAD_Q6	-719	-
SMAD_Q6	-697	-
SMAD_Q6	-278	+
SMAD_Q6	+1422	-
SMAD_Q6	+1462	-
SMAD_Q6_01	-987	-
SMAD_Q6_01	-790	+
SMAD_Q6_01	-720	-
SMAD_Q6_01	+1423	-

References

1. Csankovszki G, Nagy A, Jaenisch R (2001) Synergism of Xist RNA, DNA methylation, and histone hypoacetylation in maintaining X chromosome inactivation. *J Cell Biol* 153:773–784.
2. Komura J, Sheardown SA, Brockdorff N, Singer-Sam J, Riggs AD (1997) In vivo ultraviolet and dimethyl sulfate footprinting of the 5' region of the expressed and silent Xist alleles. *J Biol Chem* 272:10975–10980.
3. Marchetto MC*, et al.* (2010) A model for neural development and treatment of Rett syndrome using human induced pluripotent stem cells. *Cell* 143:527–539.
4. Samuelson LC, Metzger JM (2006) Isolation and freezing of primary mouse embryonic fibroblasts (MEF) for feeder plates. *CSH Protoc* 2006(2).
5. Lyst MJ*, et al.* (2013) Rett syndrome mutations abolish the interaction of MeCP2 with the NCoR/SMRT co-repressor. *Nature Neurosci* 16:898–902.
6. Ohhata T, Hoki Y, Sasaki H, Sado T (2008) Crucial role of antisense transcription across the Xist promoter in Tsix-mediated Xist chromatin modification. *Development* 135:227–235.
7. Bhatnagar S*, et al.* (2014) Genetic and pharmacological reactivation of the mammalian inactive X chromosome. *Proc Natl Acad Sci USA* 111:12591–12598.
8. Zhao W*, et al.* (2014) A New Bliss Independence Model to Analyze Drug Combination Data. *J Biomol Screen* 19:817–821.
9. Jensen EC (2013) Quantitative analysis of histological staining and fluorescence using ImageJ. *Anat Rec (Hoboken)* 296:378–381.
10. Lee TY, Chang WC, Hsu JB, Chang TH, Shien DM (2012) GPMiner: an integrated system for mining combinatorial cis-regulatory elements in mammalian gene group. *BMC Genomics* 13 Suppl 1:S3.
11. Carpenter AE*, et al.* (2006) CellProfiler: image analysis software for identifying and quantifying cell phenotypes. *Genome Biol* 7:R100.